Optical and Quantum Communications

RLE Group
Optical and Quantum Communications Group

Academic and Research Staff
Professor Jeffrey H. Shapiro, Dr. Franco N. C. Wong, Dr. Marco Fiorentino, Dr. Dmitry Kolker

Graduate Students
Marius A. Albota, Baris I. Erkmen, Saikat Guha, Taehyun Kim, Christopher E. Kuklewicz, Onur Kuzucu, Danial Lashkari, Mohsen Razavi, Dheera Venkatraman

Visiting Graduate Student
Ingo Stork genannt Wersborg

Undergraduate Student
Chen Li

The central theme of our programs has been to advance the understanding of optical and quantum communication, radar, and sensing systems. Broadly speaking, this has entailed: (1) developing system-analytic models for important propagation, detection, and communication scenarios; (2) using these models to derive the fundamental limits on system performance; and (3) identifying, and establishing through experimentation the feasibility of, techniques and devices which can be used to approach these performance limits.

1. Quantum Information and Communication

Sponsors
Air Force Research Laboratory - Cooperative Agreement F30602-01-2-0546
Army Research Office - Grant DAAD-19-00-1-0177
Army Research Office – Grant W911NF-05-1-0197
BBN Technologies
DARPA Contract HR0011-05-C-0063
U.S. Department of Interior Contract NBCHC060072
U.S. Department of Interior Contract NBCHC00671
HP-MIT Alliance
MIT Lincoln Laboratory
NIST - Grant 60NANB5D1004
NIST - Grant 60NANB5D115
Office of Naval Research - Contract N00014-03-1-0869
Office of Naval Research - Contract N00014-02-1-0717

Project Staff
Professor Jeffrey H. Shapiro, Dr. Franco N. C. Wong, Dr. Marco Fiorentino, Marius A. Albota, Baris I. Erkmen, Saikat Guha, Taehyun Kim, Christopher E. Kuklewicz, Onur Kuzucu, Danial Lashkari, Mohsen Razavi, Ingo Stork genannt Wersborg, Dheera Venkatraman

We are embarked on research in the area of quantum information technology whose goal is to enable the quantum-mechanical information transmission, storage, and processing needed for future applications in quantum computing and quantum communication. Our theoretical work in this area has focused on architectural designs for long-distance teleportation and multi-party entanglement transmission, and on novel applications of entanglement. Of particular interest has

been the identification of high-performance means for generating the polarization-entangled photons needed for many quantum information applications, including teleportation, entanglement-based quantum positioning and clock synchronization, and quantum secret sharing. We are also interested in the fundamental limits on classical information transmission that are due to the quantum noise of Bosonic channels. Our main experimental work is focused on generation and application of entanglement sources with high brightness and wavelength tunability. In addition, we are interested in novel entanglement sources and their applications in quantum logic gates, enhanced quantum measurements, and quantum teleportation protocols.

Architectural Analysis The preeminent obstacle to the development of quantum information technology is the difficulty of transmitting quantum information over noisy and lossy quantum communication channels, recovering and refreshing the quantum information that is received, and then storing it in a reliable quantum memory. We led a team of researchers from MIT and Northwestern University (NU) that proposed, analyzed, and worked to develop the key technological elements of a novel architecture for the singlet-state approach to quantum teleportation [1,2]. A simple block diagram of this architecture is shown in Fig. 1. It consists of an ultrabright narrowband source of polarization-entangled photons pairs (*P*), connected to a pair of trapped Rb atom quantum memories (*M*) by transmission through *L*-km-long lengths of standard telecommunication fiber.

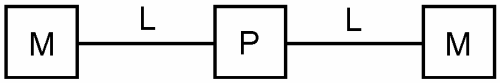

Figure 1. Schematic of long-distance quantum communication system: *P* = ultrabright narrowband source of polarization-entangled photon pairs; *L* = *L* km of standard telecommunication fiber; *M* = trapped atom quantum memory.

Each *M* block in Fig. 1 is a quantum memory in which a single ultracold ^{87}Rb atom is confined by a CO_2-laser trap in an ultra-high vacuum chamber with cryogenic walls within a high-finesse single-ended optical cavity. An abstract representation of the relevant hyperfine levels for such a memory is given in Fig. 2(a). A 795 nm photon in an arbitrary polarization can be absorbed, transferring the qubit from the photon to the degenerate *B* levels of Fig. 2(a), and thence to long-lived storage levels, by coherently driving the *B*-to-*D* transitions. By means of optically-off-resonant (OOR) transitions, the Bell states of two atoms in a single vacuum-chamber trap can be converted into superposition states of one of the atoms. All four Bell measurements needed for the Bennett *et al*. singlet-state teleportation process [3] can then be made, sequentially, by detecting the presence (or absence) of fluorescence as an appropriate sequence of OOR laser pulses is applied to the latter atom. The Bell-measurement results (two bits of classical information) in one memory can be sent to a distant memory, where (at most) two additional OOR pulses are needed to complete the state transformation process. More details on this memory, and its use in teleportation, are given in [4].

The *P* block in Fig. 1 is an ultrabright narrowband source of polarization-entangled photon pairs [5], capable of producing $\sim 10^6$ pairs/sec in $\sim$30 MHz bandwidth by appropriately combining the signal and idler output beams from two doubly-resonant type-II phase matched optical parametric amplifiers (OPAs), as sketched in Fig. 2(b). The importance of our resonant approach to entanglement generation is the need to achieve high flux within the narrow linewidth of the Rb atom memory; existing parametric downconverter sources of entanglement are far too broadband to permit useful transmission rates in the Fig. 1 architecture.

Our previous performance analysis [1,6] for the MIT/NU teleportation architecture employed cold-cavity techniques, i.e., the success probability for loading the desired singlet state into the two memories shown in Fig. 1 was found by neglecting the presence of intracavity atoms and merely calculating the probability that — at the end of a loading interval — the photon fields inside the

memory cavities are in the singlet state. During the past year we have begun to remedy the deficiency of neglecting the intracavity atoms in assessing the MIT/NU teleportation architecture [7]. A summary of the results we have obtained so far is as follows.

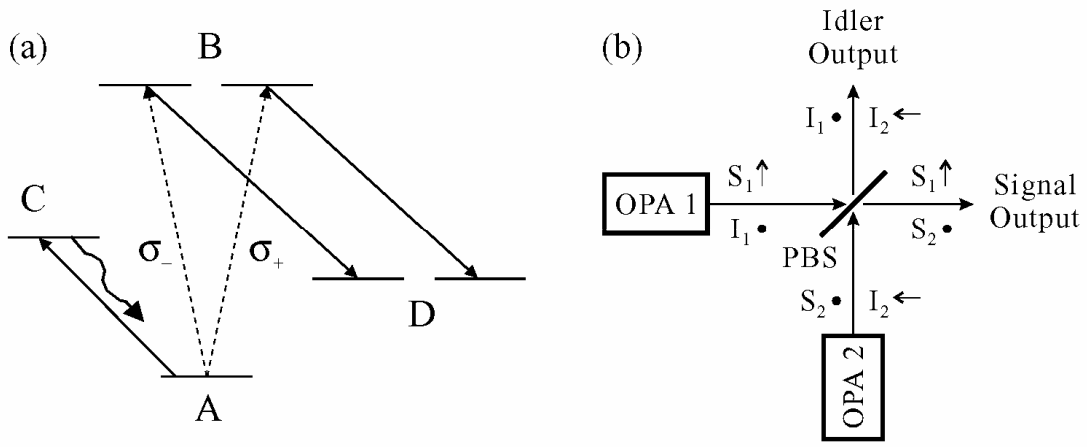

Figure 2. Essential components of singlet-state quantum communication system from Fig. 1. Left (a), simplified atomic-level schematic of the trapped Rb atom quantum memory: *A*-to-*B* transition occurs when one photon from an entangled pair is absorbed; *B*-to-*D* transition is coherently driven to enable storage in the long-lived *D* levels; *A*-to-*C* cycling transition permits nondestructive determination of when a photon has been absorbed. Right (b), ultrabright narrowband source of polarization-entangled photon pairs: each optical parametric amplifier (OPA1 and OPA2) is type-II phase matched; for each optical beam the propagation direction is *z*, and *x* and *y* polarizations are denoted by arrows and bullets, respectively; PBS, polarizing beam splitter.

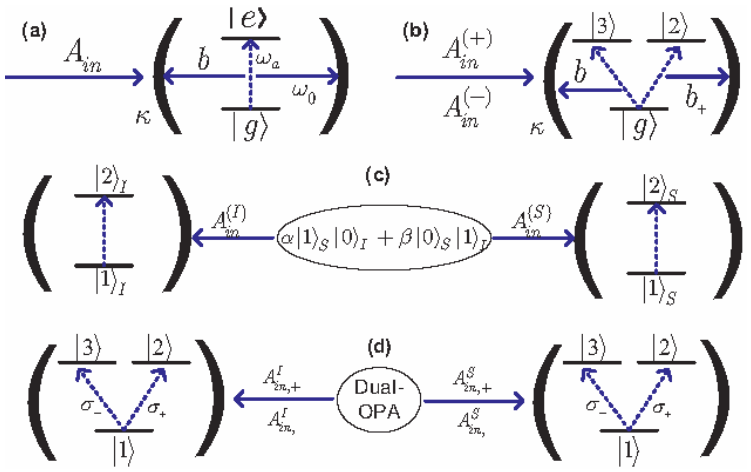

Figure 3. Trapped-atom quantum memories: (a) a two-level atom illuminated by a single photon; (b) a *V*-level atom illuminated by a single photon with an arbitrary polarization; (c) a pair of two-level atoms suitable for storing photon-number entanglement; and (d) a pair of *V*-level atoms suitable for storing polarization entanglement. All cavities are single ended.

We have considered the hierarchy of trapped-atom memory loading problems shown in Fig. 3. For a two-level atom in a single-ended cavity that is driven by an appropriately polarized single-photon excitation, as shown in Fig. 3(a), we have developed a Heisenberg-Langevin analysis that predicts the probability of successful loading of the photon into the atom as a function of the atom-field coupling, the cavity decay rate, and the single-photon pulse shape. The loading statistics for the *V*-level atom shown in Fig. 3(b), under illumination by an arbitrarily polarized

single-photon pulse, were then obtained by decomposing the problem into a pair of independent two-level atom loading problems. Likewise, the loading statistics for a pair of remotely-located two-level atoms shown in Fig. 3(c), under illumination by an appropriately polarized photon-number entangled field, also reduced to single-photon excitation of an equivalent two-level atom. However, the Heisenberg-Langevin analysis for the two *V*-level atoms shown in Fig. 3(d), does not simplify as readily, and yet of the Fig. 3 configurations it is the one that is most like the MIT/NU architecture. Thus, to obtain the loading statistics for the Fig. 3(d) configuration we are now pursuing a system-reservoir analysis, based on the Schrödinger equation, instead of the Heisenberg-Langevin treatment. The results of the new analysis will be reported once they are complete, for now we will summarize our loading theory for the two-level atom using Fig. 4. Here we have plotted the loading probability for on-resonance operation with an exponential pulse shape (proportional to $e^{\lambda t}$) that may either be exponentially rising ($\lambda > 0$) or decaying ($\lambda < 0$) for several values of λ/κ and κ/g, where κ is the cavity-decay rate and g is the atom-field coupling constant. From our knowledge of the cold-cavity dynamics, we might expect that only an exponentially-rising input pulse with $\lambda \approx \kappa$ can load the cavity with a high probability. [This follows from time-reversig the external field emanating from the output coupler when a single photon is initially present inside the cold cavity.] Figure 4 shows that fine tuning the system parameters permits a high loading probability to be achieved with exponentially-decaying pulses

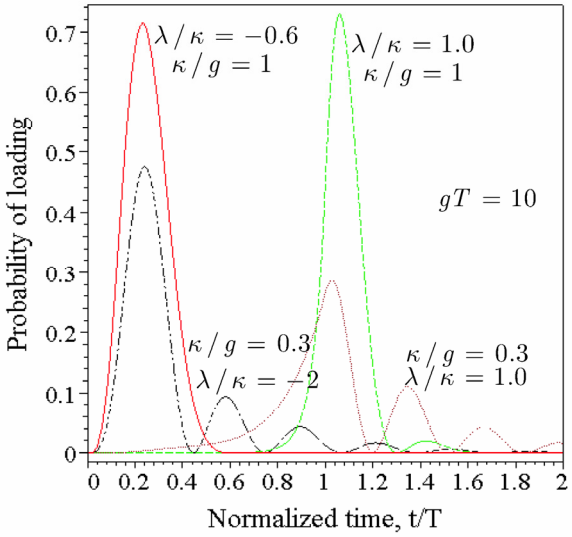

Figure 4. Time evolution of the photon-absorption probability for a two-level atom trapped in a single-ended high-*Q* cavity undergoing single-photon illumination by various exponential pulse shapes.

High-Flux Polarization Entanglement Source In recent years most entanglement sources have been based on spontaneous parametric downconversion (SPDC) in a noncollinearly propagating, angle phase-matched crystal, such as beta barium borate (BBO) [8]. We have taken a different approach to entanglement generation that takes advantage of advances in nonlinear materials and utilizes standard techniques in nonlinear optics. We employ the method of quasi-phase matching in periodically-poled potassium titanyl phosphate (PPKTP) or periodically-poled lithium niobate (PPLN) to enable efficient downconversion at user-specified wavelengths. In addition, collinear propagation of the pump, signal, and idler fields ensure easy manipulation and optimal collection of the output light. Recently we have developed the bidirectionally pumped polarization Sagnac interferometer, as shown in Fig. 5, that yields phase-stable polarization-entangled photons with high brightness and high fidelity [9].

The Sagnac source uses type-II phase-matched PPKTP as the nonlinear crystal in a compact setup that does not requires spatial, spectral, or temporal filtering. A 10-mm-long PPKTP crystal

with a 10.0-μm grating period is pumped by a fiber-coupled ultraviolet (UV) laser at 405 nm for generating polarization entanglement at 810 nm. The pump enters the Sagnac interferometer through a dual-wavelength polarizing beam splitter (PBS), which separates the pump light into its horizontal (*H*) and vertical (*V*) polarization components. The relative amplitude and phase between the pump's *H* and *V* components are set by the half-wave plate (HWP) and quarter-wave plate (QWP) placed before the interferometer. This pump control eliminates the need for pump phase stabilization that was needed in the first-generation bidirectional pumping setup using a Mach-Zehnder interferometer [10].

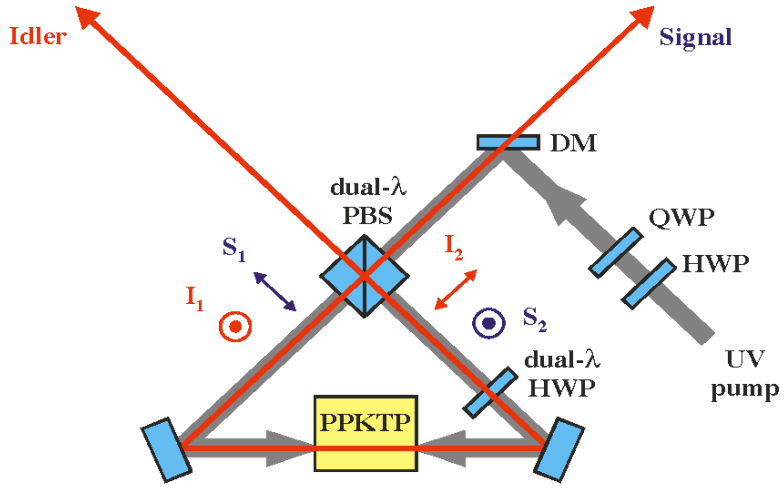

Figure 5. Schematic of bidirectionally-pumped SPDC in a Sagnac interferometer configuration. The dual-wavelength PBS combines the two downconverted outputs to form polarization-entangled signal and idler beams that may have different wavelengths. The relative amplitude and phase of the pump's *H*- and *V*-polarized components are set by the HWP and QWP. HWP, half-wave plate; QWP, quarter-wave plate; PBS, polarizing beam splitter; DM, dichroic mirror.

The PPKTP crystal is set up for frequency-degenerate type-II phase matching with orthogonally polarized signal and idler outputs. The dual-wavelength HWP rotates the *V*-polarized pump component to be *H*-polarized, along the crystal's *y* axis, which is required for SPDC in PPKTP. Bidirectional pumping thus effectively creates two identical coherently-pumped downconverters. We rotate the outputs of one of the beams by 90° with the dual-wavelength HWP, and combine the two downconverted beams at the dual-wavelength PBS, whose outputs are polarization entangled independent of the output frequencies and propagation directions. We have effectively engineered a decoherence-free subspace in which all output photon pairs are polarization entangled. There is complete indistinguishability (spatially, spectrally, and temporally) at the output. This makes it impossible to tell from which downconverter an output photon originates. Hence the output from the Fig. 5 setup is a coherent superposition of the two downconverted beams [5]. A picture of the compact setup is shown in Fig. 6. The state of the polarization-entangled output is given by

$$|\psi\rangle = \left(|H\rangle_1|V\rangle_2 - e^{i\phi}|V\rangle_1|H\rangle_2\right)/\sqrt{2},$$

where the phase ϕ is equal to the pump phase set by the pump's HWP and QWP, plus a fixed offset phase that is related to material dispersion in the interferometer. As a result, the state of the output can be precisely controlled by simply changing the relative phase between the *H*- and *V*-polarized components of the pump input.

Figure 6 shows the earlier [9] and latest [11] results of two-photon coincidence measurements for the Sagnac SPDC source output, plotting the spectral brightness as a function of the two-photon quantum interference visibility obtained at different collection-aperture sizes. By carefully optimizing the pump wavelength stability and the interferometer alignment, we have obtained a ten-fold improvement in spectral brightness at a given quantum-interference visibility: the present setup shows a flux of 9,800 pairs/s/mW of pump in a 1-nm bandwidth at 98% visibility. We have also measured the Clauser, Horne, Shimony, and Holt (CHSH) form of Bell's inequality violation [12], obtaining a value of 2.8253 ± 0.015 ± 0.0035 for the *S* parameter [11], clearly showing a strong violation of the classical limit of 2 and very close to the quantum limit of $2\sqrt{2}$. The first standard deviation of *S* is that due to systematic errors while the second standard deviation is statistical. This compact and phase-stable Sagnac source may prove to be useful for many quantum optical applications, such as quantum key distribution and linear optics quantum computing. We also intend to use the Sagnac source for the generation of hyperentangled photons that are entangled in both momentum and polarization degrees of freedom.

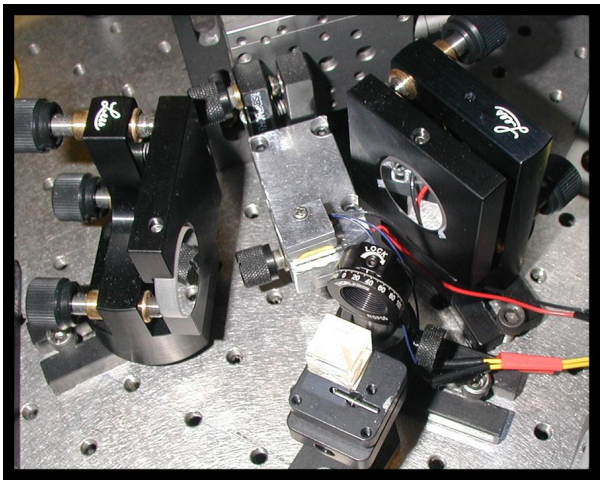

Figure 6. Bidirectionally pumped Sagnac SPDC source, showing the two flat mirrors, the crystal holder and oven, and the dual-wavelength half-wave plate and dual-wavelength polarizing beam splitter.

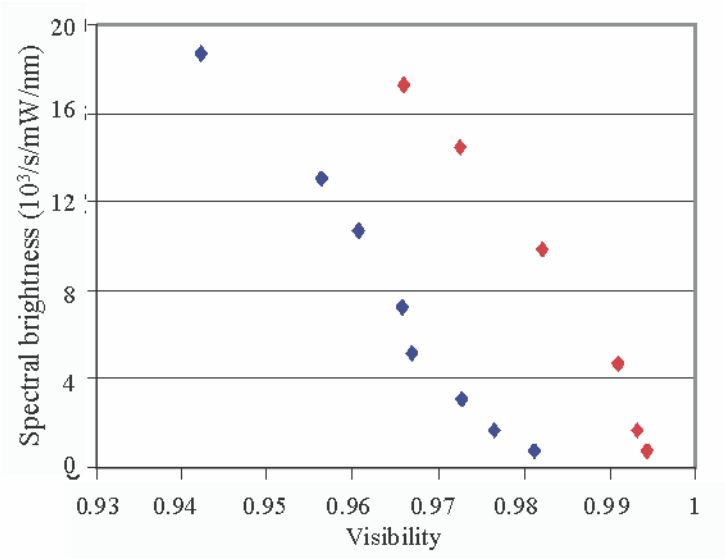

Figure 7. Comparison of spectral brightness of Sagnac source as a functon of achievable two-photon interference visibility for earlier setup (blue diamonds) [9] and improved setup (red diamonds) [11].

We have also been working on a high-flux pulsed entangment source pumped by a narrowband pulsed fiber laser source. A pulsed source of polarization-entangled photons is well suited for free-space quantum key distribution because it provides temporal discrimination against background light. We are developing a pump source at 390 nm by means of an amplified erbium-doped fiber laser at 1560 nm followed by frequency quadrupling. We have built a picosecond erbium-doped fiber ring laser using a saturable absorber mirror to provide cw passive mode locking. After amplification by a 5-W erbium-doped fiber amplifier and frequency doubling in a 10-mm-long MgO-doped PPLN crystal, we have obtained an average power of 4 W of second harmonic light at 780 nm and a conversion efficiency of ~70%. Our current task is to develop the second second-harmonic stage to generate high power UV light at 390 nm.

Cavity-Enhanced Parametric Downconversion Single-pass SPDC sources such as the Sagnac interferometer typically have large THz bandwidths that are ill-suited for coupling to the MHz bandwidth of an atomic absorption line. What is needed, to make such coupling efficient, is a bright, narrowband source of polarization-entangled photons. We have recently reported the first cavity-enhanced operation of a cw type-II downconverter, resulting in a spectrally bright, narrowband source of frequency-degenerate polarization-entangled photon pairs. More importantly, by controlling a weak intracavity birefringence, our source generates a new type of biphoton state whose polarization-entangled output is modulated between the singlet and triplet states according to the arrival-time difference between the signal and idler photons [13].

Consider a type-II phase-matched PPKTP crystal and an equal-length KTP timing compensation crystal embedded in a single-ended cavity that resonates the signal and idler, as illustrated in Fig. 8. The timing compensator ensures that the roundtrip cavity times for the orthogonally polarized signal and idler light are identical. If the signal and idler photons resulting from downconversion of a pump photon emerge from the output coupler after the same number of roundtrips within the cavity, then they yield a triplet for the post-selected biphoton state. However, the times at which these photons leave the cavity may differ by integer multiples of the cavity roundtrip time, τ_c. Taking τ_c as a natural time-bin unit for the system, we have that the biphoton state associated with a photon pair whose arrival-time difference is $m\tau_c$ is

$$|\psi\rangle = \left(|H\rangle_1|V\rangle_2 + e^{im\phi}|V\rangle_1|H\rangle_2\right)/\sqrt{2},$$

where ϕ is the roundtrip cavity birefringence. By tuning the cavity birefringence to achieve $\phi \neq 0$, we obtain a new type of biphoton, which exhibits time-bin modulated polarization entanglement. When $\phi = \pi$ and m is even, this biphoton is a triplet; when $\phi = \pi$ and m is even odd, it is a singlet.

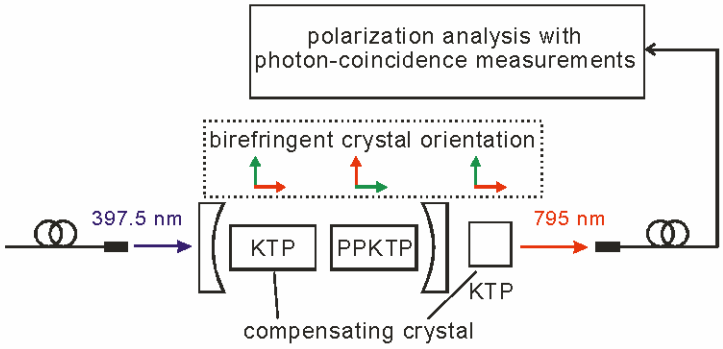

Figure 8. Schematic of cavity-enhanced parametric downconverter consisting of a single-ended optical cavity with an embedded PPKTP nonlinear crystal and an equal-length KTP timing compensator. Single-mode fiber coupling allows spatial mode filtering.

In the actual experiment shown schematically in Fig. 8, the optical cavity has a well defined spatial mode for the resonant output signal and idler light, and therefore they can be easily mode matched into a single-mode optical fiber. The fiber also acts as an excellent spatial mode filter to eliminate nonresonant SPDC outputs. The PPKTP crystal and the KTP timing compensator are temperature controlled with separate thermoelectric coolers, thus allowing the birefringence of each crystal to be fine tuned. This fine tuning capability therefore makes it possible to precisely tune the overall cavity birefringence ϕ. Figure 9 shows the results of signal and idler two-photon coincidences as a function of the cavity roundtrip difference between the two detected photons for a birefringence setting $\phi = \pi$. As expected theoretically, we observe alternating triplet and singlet quantum-interference signatures for even and odd roundtrips *m*, respectively. This novel biphoton state may be potentially useful for enhancing the security of quantum key distribution by embedding this time-bin dependent signature. Moreover, the sensitivity of the output state to cavity birefringence may find application in ultrasensitive measurements.

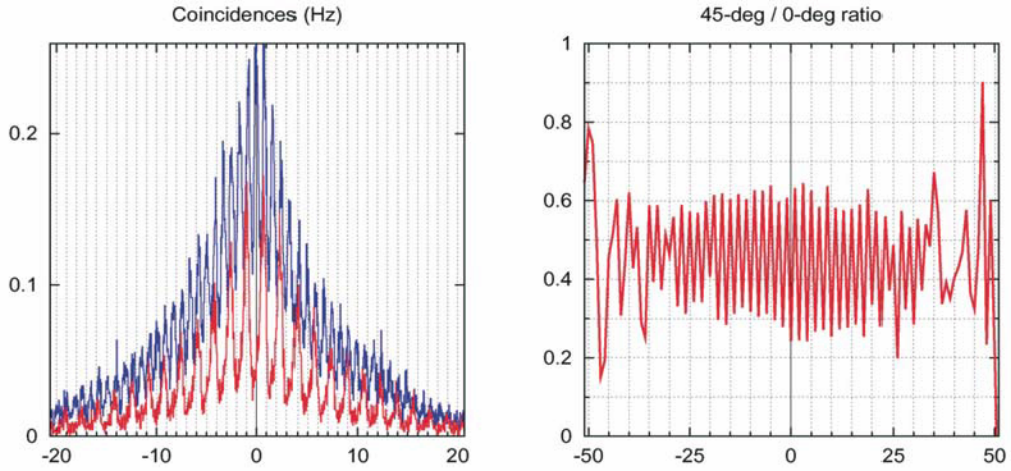

Figure 9. Left panel: two-photon coincidences as a function of signal-idler differential cavity roundtrips *m* along *H-V* polarization basis (upper blue curve) and ±45° basis (lower red curve) for cavity birefringence $\phi = \pi$. Peaks for even *m* and valleys for odd *m* correspond to time-bin modulated outputs of triplets and singlets, respectively. Right panel: normalized ratio of two-photon coincidences of upper blue curve to lower red curve of left panel. A ratio of less than 0.5 indicates quantum interference.

As a narrowband source of polarization-entangled photons, the cavity-enhanced downconverter has achieved a very high spectral brightness of 0.7 pair/s/mW of pump in 1 MHz of bandwidth in a single spatial mode [13]. In comparison, our ultrabright Sagnac source produces only 0.02 pair/s/mW in the same bandwidth for its multimode output [9]. The individual line of the broad spectral comb has an estimated bandwidth of 22 MHz, which is suitable for coupling to atom-based quantum memories. This narrowband entanglement source may be utilized for intermodal conversion between photonic qubits and atomic qubits.

Physical Simulation of the Entangling Probe BB84 Attack Fuchs and Peres [14] described the most general way in which an individual attack could be mounted against single-photon, polarization-based Bennett-Brassard 1984 quantum key distribution (BB84 QKD). Eve interacts a probe photon with Alice's photon in a unitary manner, then sends Alice's photon to Bob, and performs a probability operator-valued measurement on her probe photon. Slutsky et al. [15] demonstrated that the Fuchs-Peres construct — with the appropriate choice of probe state, interaction, and measurement — affords Eve the maximum amount of Rényi information about the error-free sifted bits that Bob receives for a given level of disturbance. Brandt [16] extended the Slutsky et al. treatment by showing that the optimal probe could be realized with a single controlled-NOT (CNOT) gate; see Fig. 10 for an abstract diagram of the resulting Fuchs-Peres-Brandt (FPB) probe. We have recently showed how a complete physical simulation of the FPB

probe could be accomplished [17] using single-photon two-qubit (SPTQ) quantum logic [18, 19]. We have made initial measurements based on SPTQ quantum logic using the setup shown in Fig. 11.

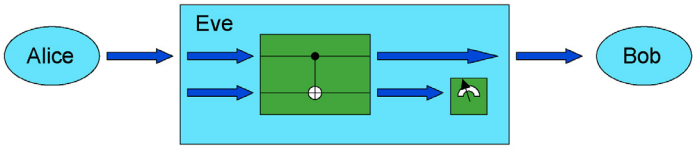

Figure 10. Fuchs-Peres-Brandt probe.

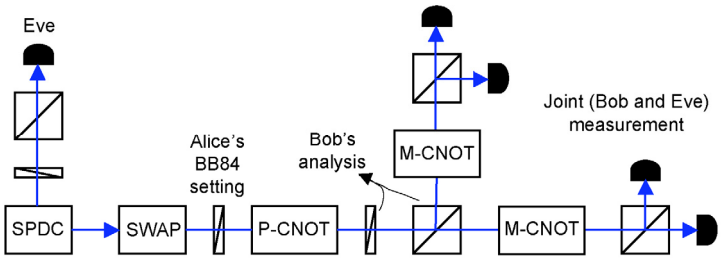

Figure 11. Physical simulation of the FPB probe.

We start with polarization-entangled photon pairs from our type-II phase matched Sagnac SPDC source [9]. Eve detects one of these photons, in a particular polarization, to both herald the presence of the other photon and determine its polarization. We then use an SPTQ SWAP gate to convert this polarization qubit into a momentum qubit, and follow that with a half-wave plate that Alice uses to set her BB84 polarization qubit. Our polarization-controlled-NOT (P-CNOT) gate then accomplishes the FPB probe interaction, with Alice's polarization qubit performing a CNOT on Eve's momentum qubit while both qubits are carried on the same photon. Another half-wave plate and a polarizing beam splitter then accomplishes Bob's active polarization analysis. At this point we use two momentum-controlled-NOT (M-CNOT) gates, a pair of polarizing beam splitters, and four single-photon detectors to collect data that allow us to determine both Bob's and Eve's measurement results under an FPB-probe attack. Because this experiment requires Eve to be inside Bob's measurement apparatus, it represents a complete physical simulation, rather than a true implementation, of the FPB-probe attack. Nevertheless, its joint Alice-Bob-Eve measurement statistics equal those of the true attack, and the latter will be realizable once polarization-independent quantum nondemolition detection becomes available [17]. Our preliminary measurements with the Fig. 11 setup have shown that Bob suffers a ~12% quantum bit error rate (QBER) when Eve sets her probe at its no-disturbance/no-information point. When she has set her probe for maximum information gain, Eve obtains ~0.9 bits/photon of information about Bob's error-free measurements while creating a ~30% QBER for Bob. We are continuing to improve on the SPTQ gate fidelities and make more detailed measurements on the FPB probe's characteristics.

Polarization-Insensitive Frequency Upconversion at 1550 nm The MIT/NU long-distance teleportation protocol depends on one's ability to efficiently translate the quantum state of a photon at ~1600 nm to 795 nm for loading the trapped-Rb quantum memory. We have demonstrated a first step toward single-photon quantum state translation by efficiently upconverting cw light at 1550 nm to 631 nm at the single photon level. Based on efficient three-wave mixing in a 4-cm-long periodically-poled lithium niobate (PPLN) crystal, a photon at 1554 nm is mixed with an intense 1064-nm-wavelength pump field, allowing it to be upconverted to 631 nm with 90% conversion efficiency [20]. This upconversion process is polarization sensitive. Only light that is polarized along the PPLN's extraordinary crystal axis is upconverted; the other polarization remains unaffected. It is desirable to achieve efficient upconversion that is not

sensitive to the polarization state, which would allow an arbitrary polarization qubit to be upconverted with polarization-state preservation.

Polarization-preserving upconversion can be achieved in a bidirectional upconversion scheme in which one polarization component is upconverted in one direction and the orthogonal polarization component in the opposite direction. A schematic is shown in Fig. 12. Consider an input with both *H* and *V* polarization components, depicted as red arrows and dots in Fig. 12. The fixed-polarization upconverter transfers only *V*-polarized light to a shorter wavelength, depicted in green. A dual-wavelength Faraday mirror rotates both the unconverted *H*-polarized light and the upconverted *V*-polarized light by 90°. On their return trip through the upconverter crystal, the *H*-polarized upconverted (green) light is not phase matched and therefore it is transmitted unchanged. The *V*-polarized unconverted (red) light is upconverted in the second pass through the upconverter. By rotating the output polarization, the input polarization state is restored in the output state at a new wavelength.

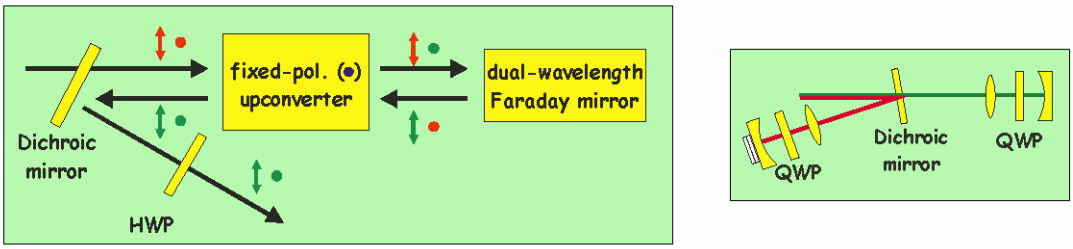

Figure 12. Schematic of polarization-insensitive upconversion. The dual-wavelength Faraday mirror is a Michelson interferometer, shown in the right panel. HWP, half-wave plate; QWP, quarter-wave plate.

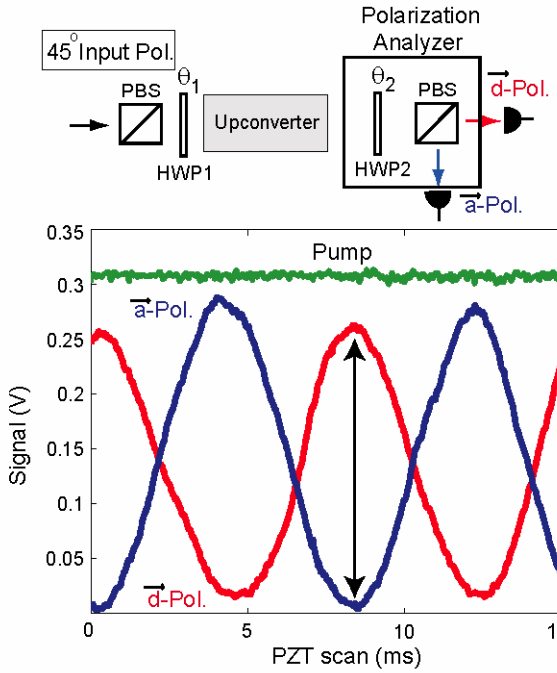

Figure 13. Output traces for the upconverted light analyzed along +45° and -45° polarizations for an input +45° polarized light. The monitored circulating pump power is also displayed. *a* and *d* polarization states refer to the anti-diagonal (-45°) and diagonal (+45°) polarization states, respectively.

In our implementation [21] a standing-wave cavity with an embedded nonlinear crystal allows upconversion to occur in both directions for a fixed polarization. A standing-wave cavity for the 1064-nm pump produces a circulating power of ~15 W from an input of ~400 mW. The dual-wavelength Faraday mirror implementation, shown in Fig. 12, right panel, uses a Michelson interferometer and a QWP-mirror combination for each wavelength. It is important that the relative phase between the unconverted and upconverted light be stabilized in order to maintain the polarization state of the input light. Moreover, the overall upconversion efficiency for both directions should be the same. Figure 16 shows the output light analyzed at ±45° for input light that is polarized at +45° with the Michelson interferometer being path stabilized, clearly demonstrating that the upconversion preserves the polarization state. For a circulating pump power of 15 W, we have reached an intrinsic upconversion efficiency of only 50% [21]. In the future, a higher pump input power or a higher finesse cavity can be used to boost the efficiency to near unity. Polarization-preserving upconversion is not only essential for quantum information processing, but it is also a valuable tool for efficient wavelength translation in many classical applications such as optical communication through the air, water, or in fiber.

Classical Capacity of Free-Space Optical Communication A principal goal of quantum information theory is evaluating the information capacities of important communication channels. At present — despite the many efforts that have been devoted to this endeavor [22] — exact capacity results are known for only a handful of channels. We have been addressing this capacity problem for a broad class of Bosonic channels, viz., those involving loss and thermal noise in both single-user and multi-user scenarios. Prior to our efforts, the major extant capacity result was for lossless — and hence noiseless — propagation [23,24]. We have derived narrowband and wideband capacity results for the single-user pure-loss Bosonic channel, in which the propagation loss — channel transmissivity $\eta<1$ — is accompanied by the minimal amount of quantum noise (vacuum-state quantum noise) that is required by quantum mechanics [25]. It turns out that the Holevo information is not superadditive for this channel, and random coding over coherent states achieves capacity. For the multiple-access channel, in which two users try to communicate simultaneously to a single receiver, we have obtained inner and outer bounds on the resulting capacity region, which are tight for the sum-rate capacity [26]. Our recent work has focused on the broadcast channel, in which one transmitter tries to simultaneously communicate different messages to a pair of receivers [27]. Here, we have built on the general theory of quantum degraded broadcast channels [28] to establish an inner bound on capacity region of the Bosonic broadcast channel. Furthermore, we have posed a minimum-output entropy conjecture that, if true, would prove that our inner bound is in fact the capacity region. This minimum output-entropy conjecture is as follows. Consider the annihilation operator beam splitter relation

$$c = \eta^{1/2} a + (1-\eta)^{1/2} b$$

in which the b mode is in its vacuum state and the a mode's state has von Neumann entropy $g(K)$, where

$$g(K) = (K+1)\log(K+1) - K\log(K)$$

is the von Neumann entropy of the thermal state with average photon number K. We conjecture that the a mode state which minimizes the von Neumann entropy of the c mode is the thermal state with average photon number K. Although we have yet to prove this minimum output-entropy conjecture, we have shown that it is true if the a mode's state is restricted to be Gaussian. We have also shown that the related conjecture for the Wehrl entropy is true.

The preceding minimum output-entropy conjecture is, in essence, the dual of the following conjecture. For the annihilation operator beam splitter relation, given above, in which the b mode is in the thermal state with average photon number N, the von Neumann entropy of the c mode is minimized when the a mode is in its vacuum state (or any other coherent state). This conjecture, for which we have a great deal of supporting evidence [29,30], has also yet to be proved. If it is true, it would show that the same coherent-state code ensemble that achieves capacity for the

pure-loss channel also achieves capacity for the thermal-noise channel [31,32]. Work is continuing on the proofs for both of these minimum output-entropy conjectures.

Phase-Conjugate Optical Coherence Tomography Optical coherence tomography (OCT) produces 3-D imagery through focused-beam scanning (for transverse resolution) and interference measurements (for axial resolution). Conventional OCT (C-OCT) uses classical-state signal and reference beams, with a phase-insensitive cross-correlation, and measures their second-order interference in a Michelson interferometer [33]. Quantum OCT (Q-OCT) employs signal and reference beams in an entangled biphoton state, and measures their fourth-order interference in a Hong-Ou-Mandel (HOM) interferometer [34,35]. In comparison to C-OCT, Q-OCT offers the advantages of a two-fold improvement in axial resolution and even-order dispersion cancellation. Q-OCT's advantages have been ascribed to the non-classical nature of the entangled biphoton state, but we have recently conceived an OCT configuration that reaps both of these advantages with classical light [37].

Q-OCT derives its signal and reference beams from spontaneous parametric downconversion (SPDC), whose outputs are in a zero-mean Gaussian state, with a non-classical phase-sensitive cross-correlation function [36]. In the low-flux limit, this non-classical Gaussian state becomes a stream of individually detectable biphotons. Classical-state light beams can also have phase-sensitive cross-correlations, but quantum or classical phase-sensitive cross-correlations do not yield second-order interference. This is why fourth-order interference is used in Q-OCT. Our new OCT configuration — phase-conjugate OCT (PC-OCT) — uses phase conjugation to convert a phase-sensitive cross-correlation into a phase-insensitive cross-correlation that can be seen in second-order interference. It turns out that phase-sensitive cross-correlation, rather than non-classical behavior *per se*, that provides the axial resolution improvement and even-order dispersion cancellation.

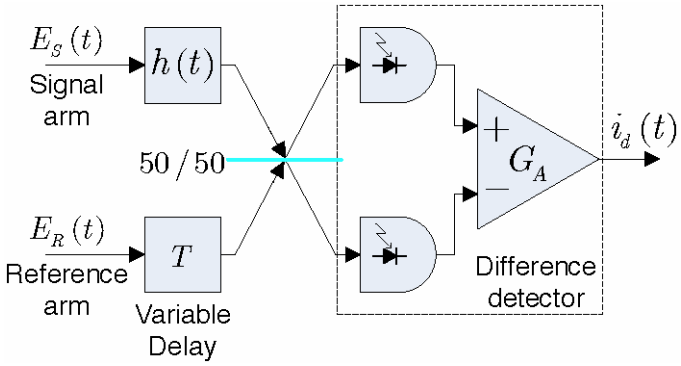

Figure 14. Schematic for conventional optical coherence tomography. The signal and reference are broadband light beams with a phase-insensitive cross correlation. The signal is transmitted to a target represented by a linear time-invariant filter $h(t)$ — shown here in transmission, but in the real application it would be seen in reflection — and then interfered with the delayed reference in a Michelson interferometer. Axial information is derived from the location of peak fringe visibility.

Figures 14 and 15 provide a comparison between C-OCT and PC-OCT. Both systems gain axial information by locating the fringe-visibility peak in a Michelson interferometer formed by the signal and reference beams. In C-OCT the signal and reference beams have a phase-insensitive cross correlation, and can be obtained by 50/50 beam splitting of the light from a single broadband source. In PC-OCT, the signal and reference beams have a phase-sensitive cross correlation, so they must be obtained as the signal and idler outputs from a phase-sensitive interaction like parametric amplification or downconversion. The major difference between C-OCT and PC-OCT is that the former interrogates the target only once — shown in Fig. 14 as a single passage through a linear time-invariant filter $h(t)$ — whereas the latter must interrogate the target twice, once before and once after a phase conjugation operation. Phase conjugation, performed in

another parametric device, converts the phase-sensitive cross correlation to a phase-insensitive cross correlation. The former cannot be measured in a second-order interferometer, like the Michelson arrangement shown in Fig. 15, whereas the latter can. Because the phase-conjugate system interrogates the target twice, its axial resolution is $c/2B$, where c is the speed of light and B is the bandwidth of the signal and reference beams. The conventional system, on the other hand, has axial resolution c/B for the same optical bandwidth. A two-pass conventional system would also achieve $c/2B$ axial resolution, but it would suffer *double* the group-velocity dispersion of the single-pass conventional system, while the phase-conjugate system enjoys dispersion cancellation. This means that PC-OCT will have at least a factor-of-two advantage over C-OCT with the same optical bandwidth.

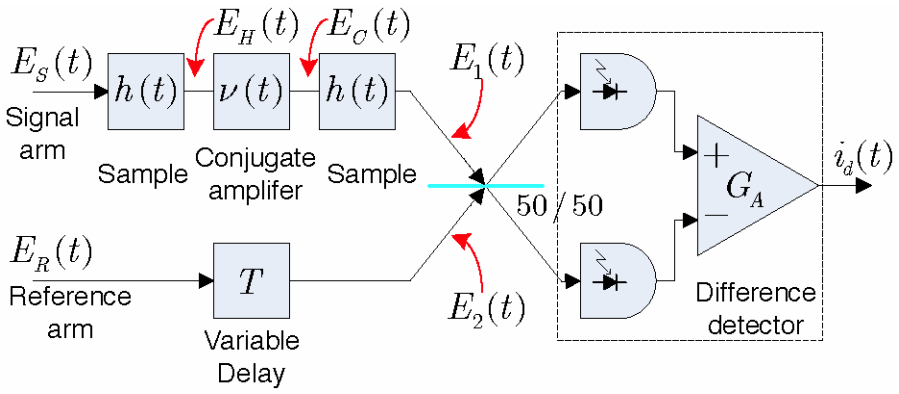

Figure 15. Schematic for phase-conjugate optical coherence tomography. The signal and reference are broadband light beams with a phase-sensitive cross correlation. The signal is transmitted to a target represented by a linear time-invariant filter $h(t)$ — shown here in transmission, but in the real application it would be seen in reflection — and then phase conjugated upon its return in a parametric device with impulse response $\nu(t)$. The conjugate beam re-interrogates the target after which it is interfered with the delayed reference in a Michelson interferometer. Axial information is derived from the location of peak fringe visibility.

2. Nonlinear Optics and Precision Measurements

Sponsor
Office of Naval Research - Contract N00014-02-1-0717

Project Staff
Professor Jeffrey H. Shapiro, Dr. Franco N. C. Wong, Dr. Dmitry Kolker

In an era that is increasingly technology driven, precision measurements play a key role in many areas of science and commerce, such as the very successful Global Positioning System (GPS). The recent introduction of femtosecond frequency-comb technology bridges the two extremes of time scales: ultrafast optics in the femtosecond regime and optical frequency metrology at the Hertz and sub-Hertz levels. One significant consequence is the functionality and simplicity afforded by femtosecond technology for use in precision measurements, such as the determination of absolute optical frequencies. We are working in collaboration with Professors Erich Ippen and Franz Kärtner to investigate enabling femtosecond-comb technologies with nonlinear optical techniques.

The main focus of our program is to apply nonlinear optical techniques to improve both the signal-to-noise ratio and stability of self-frequency referencing techniques and to facilitate new applications of femtosecond-comb technology for enhanced functionality. The technique of quasi-phase matching and the availability of multiple gratings in a single PPLN crystal offer

flexibility in achieving multiple interactions by allowing each nonlinear process to take place in its own grating section. Back-to-back difference-frequency generation in a dual-grating PPLN chip has been used to achieve optical frequency division by 3 [38]. More recently, we have realized self-phase locking in a divide-by-3 optical parametric oscillator (OPO) using a dual-grating PPLN chip in a triply resonant cavity [39].

In the past year, we have taken the concept of multiple interactions to a new level of flexibility and tunability in a convenient setup. First we incorporated a fan-out grating section in a dual-grating PPLN chip. The phase matching of the uniform-grating first section is tunable by temperature. The interaction in the second section is tunable by a simple translation of the chip across the variable-period grating without affecting the first-section phase matching. We utilized this dual-grating design to demonstrate a tunable cascaded OPO in a cavity that is resonant at all generated frequencies [40]. Pumped at 532 nm, the first grating generates the primary OPO (P-OPO) while the secondary OPO (S-OPO) is internally pumped by the primary signal field. We have experimentally demonstrated wide tunability of 200 nm in the secondary OPO outputs by translating across the fan-out section. Moreover, we have observed optical limiting for the primary signal output above the S-OPO threshold while the pump is no longer clamped. In addition, our theoretical model predicts that above S-OPO threshold the power transfer from the pump to OPO outputs, other than the clamped primary signal, is linear in power. In contrast, conventional OPOs show clamping of the pump only and a square-root power dependence.

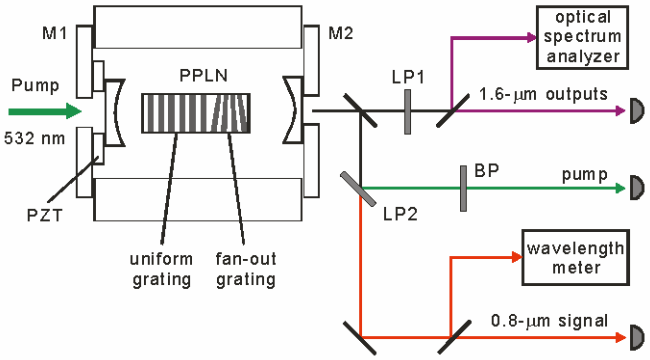

Figure 16. Schematic of experimental setup. Cascaded OPO output powers are monitored and output wavelengths are measured. LP1, 1-μm long-pass filter; LP2, 0.7-μm long-pass filter; BP, 532-nm band-pass filter; PZT, piezoelectric transducer.

Figure 16 shows the schematic of the experimental setup. The pump was a continuous-wave (cw) single-frequency 532-nm laser. We used a 20-mm-long PPLN crystal with a 13-mm first section of 7.2 μm grating period that could be phase matched for nondegenerate OPO outputs at ~0.8 and ~1.6 μm. The PPLN temperature was typically set between 150 to 220°C that allowed tunable P-OPO outputs. The PPLN chip had a 7-mm second section with a fan-out grating structure that varied from 19.45 to 19.85 μm over the 10-mm width of the crystal. At a fixed temperature, the PPLN chip could be translated along its width to access different grating periods of the fan-out section without changing the phase-matching condition for the P-OPO. The fan-out structure was used for phase-matched parametric generation of tunable outputs centered around 1.6 μm when pumped by the primary signal at 0.8 μm.

Figure 17 plots the cascaded OPO output wavelengths centered around the 1.6 μm region, consisting of the primary idler at 1600 nm, and the secondary signal and idler as a function of the grating location of the fan-out section of the PPLN crystal. The wavelength coverage, including the primary idler, spans ~200 nm with a fixed pump wavelength of 532 nm and at a fixed temperature. Figure 18 shows the power dependence of the cascaded OPO as a function of

input pump power. Except for the lowest pump power, at which the S-OPO was below threshold, we observe that the primary signal power is clamped and the output pump and 1.6 μm have linear power dependence as clearly indicated by the linear fits to the data.

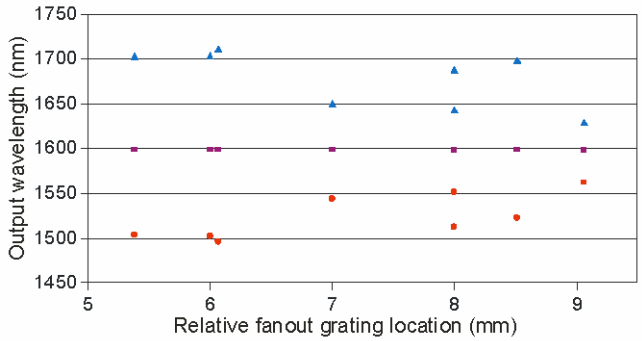

Figure 17. Output wavelengths versus fan-out grating location. Operating temperature: 204°C.

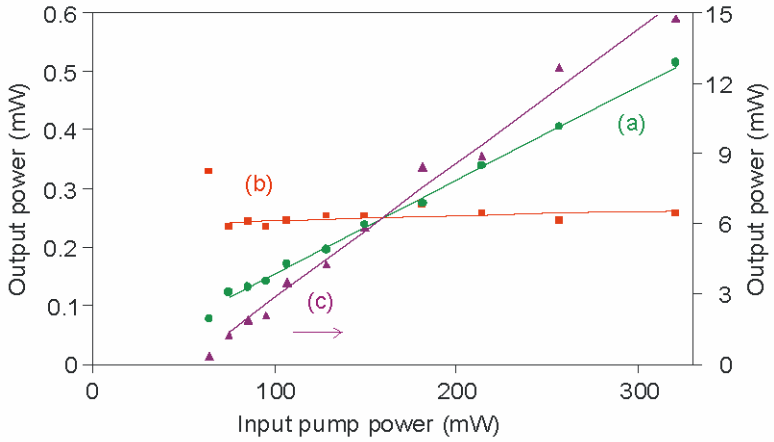

Figure 18. Plot of (a) pump (green circles), (b) signal (orange squares), and (c) 1.6-μm output (purple triangles) powers versus input pump power. The S-OPO was above threshold except for data taken at 64 mW which are excluded for the linear fits (solid lines), showing clamping of the primary signal, and linear output powers for the pump, primary idler, and S-OPO outputs..

In addition to the demonstration of cascaded optical parametric oscillation, we will be studying the dual-grating OPO to observe self-phase locking in which the second harmonic of the idler is self-phase locked to the signal field, yielding precise 3-to-1 frequency division. A self-phase locked 3-to-1 OPO is particularly interesting because its three frequency markers can be utilized to phase lock two femtosecond frequency combs in different spectral regions to form a single multi-octave frequency comb for precision frequency metrology applications.

References

1. J. H. Shapiro, "Architectures for Long-Distance Quantum Communication," *New J. Phys*. 4, 47.1-47.18 (2002).

2. S. Lloyd, J. H. Shapiro, F. N. C. Wong, P. Kumar, S. M. Shahriar, and H. P. Yuen, "Infrastructure for the Quantum Internet," ACM SIGCOMM *Comp. Commun. Rev.* 34, 9-20 (2004).

3. C. H. Bennett, G. Brassard, C. Crépeau, R. Jozsa, A. Peres, and W. K. Wootters, "Teleporting and Unknown Quantum State via Dual Classical and Einstein-Podolsky-Rosen Channels," *Phys. Rev. Lett*. 70, 1895-1899 (1993).

4. S. Lloyd, M. S. Shahriar, J. H. Shapiro, and P. R. Hemmer, "Long-Distance Unconditional Teleportation of Atomic States via Complete Bell State Measurements," *Phys. Rev. Lett*. 87, 167903 (2001).

5. J. H. Shapiro and N. C. Wong, "An Ultrabright Narrowband Source of Polarization-Entangled Photon Pairs," *J. Opt. B: Quantum Semiclass*. *Opt*. 2, L1-L4 (2000).

6. B. J. Yen and J. H. Shapiro, "Error Models for Long-Distance Qubit Teleportation," IEEE *J. Sel. Topics in Quantum Electron*. 9, 1483-1494 (2003).

7. M. Razavi, V. Giovannett, L. Maccone, and J. H. Shapiro, "Hot-Cavity Loading: a Heisenberg-Langevin Analysis," *Digest of Quantum Electronics and Laser Science Conference*, Long Bech, California, May 21-26, 2006.

8. P. G. Kwiat, E. Waks, A. G. White, I. Appelbaum, and P. H. Eberhard, "Ultrabright Source of Polarization-Entangled Photons," *Phys. Rev. A* 60, R773-R776 (1999).

9. T. Kim, M. Fiorentino, and F. N. C. Wong, "Phase-Stable Source of Polarization-Entangled Photons using a Polarization Sagnac Interferometer," *Phys. Rev. A* 73, 012316 (2006).

10. M. Fiorentino, G. Messin, C. E. Kuklewicz, F. N. C. Wong, and J. H. Shapiro, "Generation of Ultrabright Tunable Polarization Entanglement without Spatial, Spectral or Temporal Constraints," *Phys. Rev. A* 69, 041801(R) (2004).

11. F. N. C. Wong, J. H. Shapiro, and T. Kim, "Efficient Generation of Polarization-Entangled Photons in a Nonlinear Crystal," *Laser Phys.,* forthcoming (2006).

12. J. F. Clauser, M. A. Horne, A. Shimony, and R. A. Holt, "Proposed Experiment to Test Local Hidden-Variable Theories," *Phys. Rev. Lett.* 23, 880-884 (1969).

13. C. E. Kuklewicz, F. N. C. Wong, and J. H. Shapiro, "Time-Bin Modulated Polarization-Entangled Biphotons from Cavity-Enhanced Down-Conversion," quant-ph/0605093.

14. C. A. Fuchs and A. Peres, "Quantum-State Disturbance versus Information Gain: Uncertainty Relations for Quantum Information," *Phys. Rev. A* 53, 2038-2045 (1996).

15. B. A Slutsky, R. Rao, P.-C. Sun, and Y. Fainman, "Security of Quantum Cryptography against Individual," *Phys. Rev. A* 57, 2383-2398 (1998).

16. H. E. Brandt, "Quantum-Cryptographic Entangling Probe," *Phys. Rev. A* 71, 042312 (2005).

17. J. H. Shapiro and F. N. C. Wong, "Attacking Quantum Key Distribution with Single-Photon Two-Qubit Quantum Logic," *Phys. Rev. A* 73, 012315 (2006).

18. M. Fiorentino and F. N. C. Wong, “Deterministic Controlled-NOT Gate for Single-Photon Two-Qubit Quantum Logic,” *Phys. Rev. Lett.* 93, 070502 (2004).

19. M. Fiorentino, T. Kim, and F. N. C. Wong, “Single-Photon Two-Qubit SWAP Gate for Entanglement Manipulation,” *Phys. Rev. A* 72, 012318 (2005).

20. M. A. Albota and F. N. C. Wong, “Efficient Single-Photon Counting at 1.55 μm by means of Frequency Upconversion,” *Opt. Lett*. 29, 1449-1451 (2004).

21. M. A. Albota, F. N. C. Wong, and J. H. Shapiro, “Polarization-Independent Frequency Conversion for Quantum Optical Communication,” *J. Opt. Soc. Am. B* 23, 918-924 (2006).

22. C. H. Bennett and P. W. Shor, “Quantum Information Theory,” *IEEE Trans. Information Theory* 44, 2724-2742 (1998), and references therein.

23. H. P. Yuen and M. Ozawa, “Ultimate Information Carrying Limit of Quantum Systems,” *Phys. Rev. Lett*. 70, 363-366 (1993).

24. C. M. Caves and P. D. Drummond, “Quantum Limits on Bosonic Communication Rates,” *Rev. Mod. Phys.* 66, 481-537 (1994).

25. V. Giovannetti, S. Guha, S. Lloyd, L. Maccone, J. H. Shapiro, and H. P. Yuen, “Classical Capacity of the Lossy Bosonic Channel: the Exact Solution,” *Phys. Rev. Lett*. 92, 027902 (2004).

26. B. J. Yen and J. H. Shapiro, “Multiple-Access Bosonic Communications,” submitted to *Phys. Rev. A* 72, 062312 (2005).

27. S. Guha and J. H. Shapiro, “Bosonic Broadcast Channel Capacity and a New Minimum Output Entropy Conjecture,” to be presented at the *Eighth International Conference on Quantum Communication, Measurement and Computing*, Tsukuba, Japan, November 28 – December 3, 2006.

28. J. Yard, P. Hayden, and I. Devetak, “Quantum Broadcast Channels,” e-print quant-ph/0603098.

29. V. Giovannetti, S. Guha, S. Lloyd, L. Maccone, and J. H. Shapiro, “Minimum Output Entropy of Bosonic Channels: a Conjecture,” *Phys. Rev. A* 70, 032315 (2004).

30. V. Giovannetti, S. Lloyd, L. Maccone, J. H. Shapiro, and B. J. Yen, “Minimum Rényi and Wehrl Entropies at the Output of Bosonic Channels,” *Phys. Rev. A* 70, 022328 (2004).

31. V. Giovannetti, S. Guha, S. Lloyd, L. Maccone, J. H. Shapiro, B. J. Yen, and H. P. Yuen, “Classical Capacity of Free-Space Optical Communication,” *Quant. Inform. and Comput*. 4, 489-499 (2004).

32. J. H. Shapiro, V. Giovannetti, S. Guha, S. Lloyd, L. Maccone, and B. J. Yen, “Capacity of Bosonic Communications,” in *Proceedings of the Seventh International Conference on Quantum Communication, Measurement and Computing*, eds. S. M. Barnett, E. Anderson, J. Jeffers, P. Öhberg, and O. Hirota (American Institute of Physics, 2004).

33. J. M. Schmitt, “Optical Coherence Tomography: A Review,” *J. Sel. Top. In Quantum Electron*. 5, 1205-1215 (1999).

34. A. F. Abouraddy, M. B. Nasr, B. E. A. Saleh, A. V. Sergienko, and M. C. Teich, "Quantum Optical Coehrence Tomography with Disperion Cancellation," *Phys. Rev. A* 65 053817 (2002).

35. M. B. Nasr, B. E. A. Saleh, A. V. Sergienko, and M. C. Teich, "Demonstration of Dispersion-Canceled Quantum-Optical Coherence Tomography," *Phys. Rev. Lett*. 91, 083601 (2003).

36. J. H. Shapiro and K.-X. Sun, "Semiclassical versus Quantum Behavior in Fourth-Order Interference," *J. Opt. Soc. Am. B* 11, 1130-1141 (1994).

37. B. I. Erkmen and J. H. Shapiro, "Phase-Conjugate Optical Coherence Tomography," submitted to *Phys. Rev. A*; e-print quant-ph/0607125.

38. P. T. Nee and N. C. Wong, "Optical Frequency Division by 3 of 532 nm in Periodically Poled Lithium Niobate with a Double Grating," *Opt. Lett.* 23, 46-48 (1998).

39. J.-J. Zondy, D. Kolker, and F. N. C. Wong, "Dynamical Signatures of Self-Phase-Locking in a Triply Resonant Optical Parametric Oscillator," *Phys. Rev. Lett.* 93, 043902 (2004).

40. P. V. Gorelik, F. N. C. Wong, D. Kolker, J.-J. Zondy, "Cascaded Optical Parametric Oscillation with a Dual-Grating Periodically Poled Lithium Niobate Crystal," *Opt. Lett.* 31, 2039-2041 (2006).

Publications

Journal Articles, Published

M. Fiorentino, T. Kim, and F. N. C. Wong, "Single-Photon Two-Qubit SWAP Gate for Entanglement Manipulation," *Phys. Rev. A* 72, 012318 (2005).

J. H. Shapiro, S. Guha, and B. I. Erkmen, "Ultimate Channel Capacity of Free-Space Optical Communications," *J. Opt. Networking* 4, 505-516 (2005).

B. J. Yen and J. H. Shapiro, "Multiple-Access Bosonic Communications," *Phys. Rev. A* 72, 062312 (2005).

J. H. Shapiro and F. N. C. Wong, "Attacking Quantum Key Distribution with Single-Photon Two-Qubit Quantum Logic," *Phys. Rev. A* 73, 012315 (2006).

T. Kim, M. Fiorentino, and F. N. C. Wong, "Phase-Stable Source of Polarization-Entangled Photons using a Polarization Sagnac Interferometer," *Phys. Rev. A* 73, 012316 (2006).

J. H. Shapiro, "Performance Analysis for Brandt's Conclusive Entangling Probe," Quantum Inform. Process. 5, 11–24 (2006).

M. Razavi and J. H. Shapiro, "Long-Distance Quantum Communication with Neutral Atoms," Phys. Rev. A 73, 042303 (2006).

M. A. Albota, F. N. C. Wong, and J. H. Shapiro, "Polarization-Independent Frequency Conversion for Quantum Optical Communication," *J. Opt. Soc. Am. B* 23, 918-924 (2006).

P. V. Gorelik, F. N. C. Wong, D. Kolker, J.-J. Zondy, "Cascaded Optical Parametric Oscillation with a Dual-Grating Periodically Poled Lithium Niobate Crystal," *Opt. Lett.* 31, 2039-2041 (2006).

Journal Articles, Accepted for Publication

F. N. C. Wong, J. H. Shapiro, and T. Kim, “Efficient Generation of Polarization-Entangled Photons in a Nonlinear Crystal,” *Laser Phys.,* forthcoming (2006).

Journal Articles, Submitted for Publication

C. E. Kuklewicz, F. N. C. Wong, and J. H. Shapiro, “Time-Bin Modulated Polarization-Entangled Biphotons from Cavity-Enhanced Down-Conversion,” submitted to *Phys. Rev. A*; e-print quant-ph/0605093.

B. I. Erkmen and J. H. Shapiro, “Phase-Conjugate Optical Coherence Tomography,” submitted to *Phys. Rev. A*; e-print quant-ph/0607125.

Meeting Papers, Published

J. H. Shapiro and F. N. C. Wong, “Attacking Quantum Key Distribution with Single-Photon Two-Qubit Quantum Logic,” *Digest of Quantum Electronics and Laser Science Conference*, Long Beach, California, May 21-26, 2006.

J. H. Shapiro and R. S. Bondurant, "Qubit Degradation due to Cross-Phase Modulation Photon-Number Measurement," *Digest of Quantum Electronics and Laser Science Conference*, Long Beach, California, May 21-26, 2006.

C.E. Kuklewicz, F. N. C. Wong, and J. H. Shapiro, “Novel Time-Bin Dependent Polarization Entanglement via Cavity-Phase Control,” *Digest of Quantum Electronics and Laser Science Conference*, Long Beach, California, May 21-26, 2006.

P. V. Gorelik, F. N. C. Wong, D. Kolker, and J.-J. Zondy, “Cascaded Optical Parametric Oscillation using a Dual-Grating PPLN Crystal,” *Digest of Conference on Lasers and Electro-Optics*, Long Beach, California, May 21-26, 2006.

T. Kim, M. Fiorentino, and F. N. C. Wong, “Phase-Stable Source of Polarization-Entangled Photons using a Polarization Sagnac Interferometer,” *Digest of Quantum Electronics and Laser Science Conference*, Long Beach, California, May 21-26, 2006.

M. Razavi, V. Giovannetti, L. Maccone, and J. H. Shapiro, "Hot-Cavity Loading: a Heisenberg-Langevin Analysis," *Digest of Quantum Electronics and Laser Science Conference*, Long Beach, California, May 21-26, 2006.

Theses

C. E. Kuklewicz, *Ultrabright Source of Polarization-Entangled Photons from Cavity-Enhanced Downconversion,* Ph.D. diss., Department of Physics, MIT 2005; also Res. Lab. Electron. Technical Rep. 713.

M. A. Albota, *Single-Photon Frequency Upconversion for Long-Distance Quantum Teleportation and Communication,* Ph.D. diss., Department of Electrical Engineering and Computer Science, MIT 2006; also Res. Lab. Electron. Technical Rep. 714.